

Hydrodynamics of a Semipermeable Vesicle Under Flow and Confinement

Bryan Quaife^a, Ashley Gannon^a, and Y.-N. Young^{b,1}

^aDepartment of Scientific Computing, Florida State University, Tallahassee, FL 32306; ^bDepartment of Mathematical Sciences, New Jersey Institute of Technology, Newark, NJ 07102

This manuscript was compiled on February 1, 2022

Lipid bilayer membranes have a native (albeit small) permeability for water molecules. Under an external load, provided that the bilayer structure stays intact and does not suffer from poration or rupture, a lipid membrane deforms and its water influx/efflux is often assumed negligible in the absence of osmolarity. In this work we use boundary integral simulations to investigate the effects of water permeability on the vesicle hydrodynamics due to a mechanical load, such as the viscous stress from an external flow deforming a vesicle membrane in free space or pushing it through a confinement. Incorporating the membrane permeability into the framework of Helfrich free energy for an inextensible, elastic membrane as a model for a semipermeable vesicle, we illustrate that, in the absence of an osmotic stress gradient, the semipermeable vesicle is affected by water influx/efflux over a sufficiently long time or under a strong confinement. Our simulations quantify the conditions for water permeation to be negligible in terms of the time scales, flow strength, and confinement. These results shed light on how microfluidic confinement can be utilized to estimate membrane permeability.

Semipermeable membrane | Vesicle | Extreme confinement | Boundary integral equations | Stokes flow

Water exchange is essential for a living cell to adapt to its environment over a wide range of time scales (1–9). Recent findings confirm that both osmotic and mechanical stresses contribute to significant water permeation for cells to migrate under strong confinement (10–13), leading to a dynamic surface-to-volume ratio of a migrating cell. While stress-induced release of messengers in cells has been well-studied (14–18), mechanically induced water permeation is often associated with membrane poration or rupture under extreme stresses (19, 20). In this work we use modeling and direct numerical simulations to show that, over the appropriate time scales or under strong confinement, the intrinsic membrane permeability to water can give rise to significantly distinct hydrodynamics of a semipermeable vesicle without poration or rupture in the lipid bilayer membrane.

The lipid bilayer membrane is permeable to water and lipid-soluble molecules (21–24). In the red blood cell membrane, aquaporin-1 channels give rise to a much higher water permeability coefficient of approximately 1.8×10^{-2} cm/s in erythrocytes (3) while the intrinsic water permeability of a lipid bilayer membrane is in the range of 10^{-4} – 10^{-3} cm/s (22, 24–27). Without aquaporins or other membrane channels that promote water permeability, the intrinsic membrane permeability is known to depend on the temperature, lipid composition (28), and the hydration of the membrane (29). Molecular dynamic (MD) simulations show that a stretched red blood cell membrane porates when the membrane tension reaches the order of 2–4 mN/m ((20) and references therein), giving rise to enhanced membrane permeability to both water and

macromolecules. Consequently, as long as the lipid bilayer membrane remains intact (no poration or rupture), the total amount of water inside the membrane is assumed constant throughout the experiment of duration no longer than tens of minutes. Under what condition is this a good assumption? Do liposomes conserve volume under flow over a long time (hours)? What is the dynamic consequence when water influx/efflux affects the membrane hydrodynamics? To answer these questions, we investigate the balance between hydrodynamics stresses, tension, and elastic stress of a semipermeable membrane under various flowing conditions and confinement (Figure 1).

Vesicles have been used as a model system to study reshaping, remodeling, and scission of cell membranes due to osmotic stress (26, 27, 30–32). These results illustrate that the permeating water flow is inevitably coupled with the mechanical pressure jump across the membrane (13), which could become comparable to osmotic stress when the membrane deformation is large (12, 13). In microfluidic experiments, it is challenging to keep a freely suspended red blood cell or vesicle in a steady flow for more than a few hours. It is also difficult to quantify the vesicle surface-to-volume ratio accurately (33). Using numerical simulations we can quantify the effects of water permeability on the hydrodynamics of a vesicle under mechanical stresses. Without an osmotic gradient, we first show that a freely suspended semipermeable vesicle behaves differently from an impermeable vesicle over a long time. Next we show that the permeating water flow can be amplified by extreme confinement to give rise to observable change in both hydrodynamics and water content. These results provide insight into quantifying the effects of membrane permeability on vesicle hydrodynamics in microfluidics.

Formulation

We consider a two-dimensional semipermeable vesicle (permeable only to water) suspended in a viscous fluid (Figure 1), and we let γ denote the membrane boundary. We let $\alpha = 4\pi A/L^2$ be the vesicle’s reduced area where A is its area and L is its length. To focus on the effect of water flow on vesicle hydrodynamics in various conditions, we assume the fluid is the same inside and outside the vesicle membrane. On the membrane the permeable water flux gives rise to a difference between the fluid velocity $\mathbf{u}(\mathbf{x} \in \gamma)$ and the membrane velocity $\dot{\mathbf{x}}$ (13):

$$\mathbf{u} - \dot{\mathbf{x}} = -k_w(RT\Delta c + \mathbf{f}_{\text{mem}} \cdot \mathbf{n}), \quad \mathbf{x} \in \gamma, \quad [1]$$

B.Q. and Y.-N.Y. designed and performed research with A.G.’s assistance. B.Q. and Y.-N.Y. analyzed the data and wrote the paper.

¹ Corresponding author’s e-mail: yyoung@njit.edu

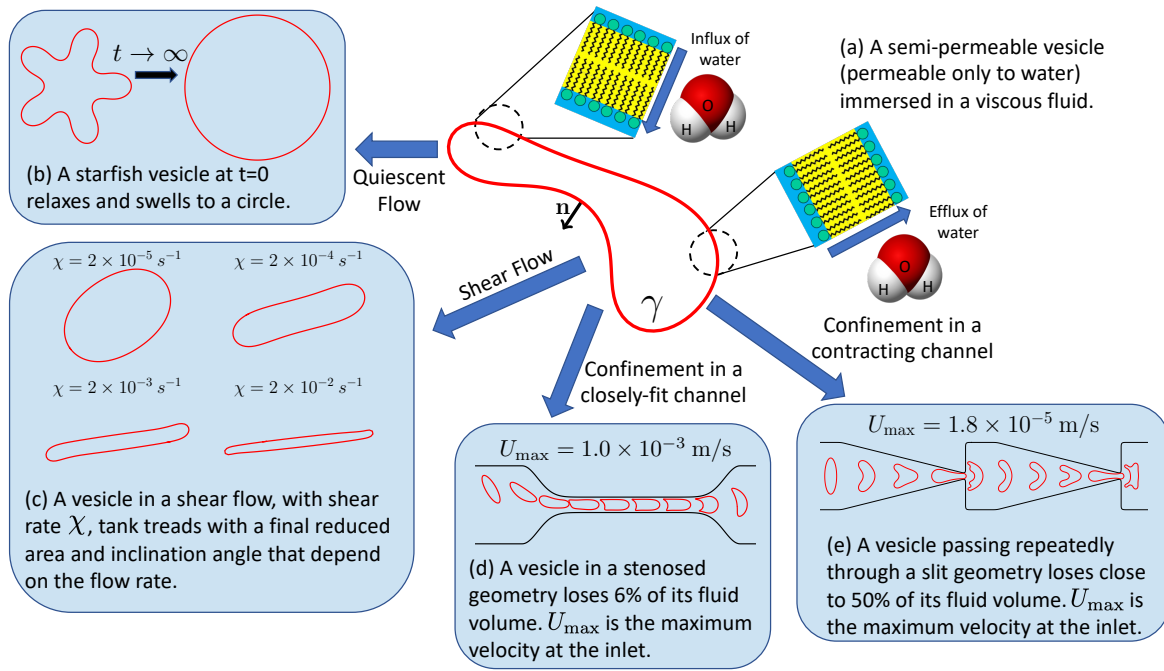


Fig. 1. Schematics showing the effects of semipermeability on vesicle hydrodynamics in various configurations. The lipid bilayer membrane (modeled as an interface γ of zero thickness and an outward normal \mathbf{n}) is permeable to water molecules, depending on the mechanical normal stress balance on the membrane. The slipper in (a) is the steady-state shape of a semipermeable vesicle in a Poiseuille flow.

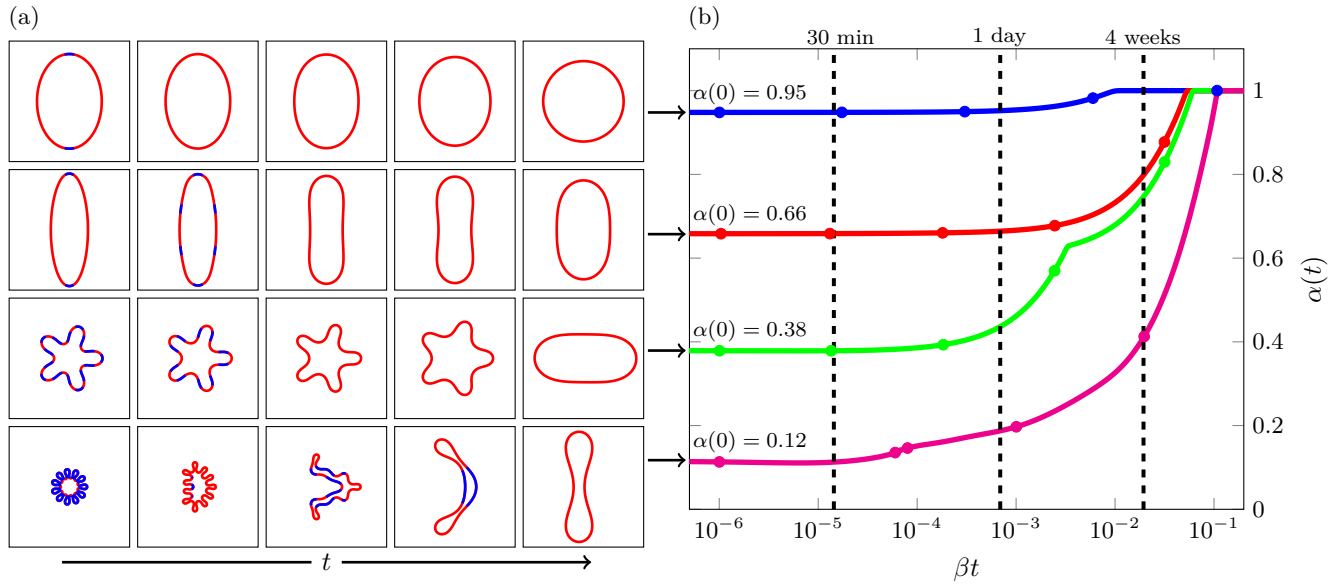


Fig. 2. (a) Snapshots of four semipermeable vesicles with $\beta = 10^{-8}$ submerged in a fluid with no background flow. Time goes from left to right. The red regions correspond to influx and the blue regions correspond to efflux. In all cases, the vesicle reaches a steady state circular shape. (b) The reduced area of each of the simulations. The particular snapshots in (a) occur at the marks along the curve.

where \mathbf{n} is the outward normal (Figure 1), k_w is the hydraulic conductivity ($\text{m}^2\text{s/kg}$), R is the ideal gas constant, T is the temperature (K), Δc is contrast in a solute concentration (mol/volume), and \mathbf{f}_{mem} is the membrane stress that consists of both bending $\mathbf{f}_{\text{ben}} = -k_b \mathbf{x}_{ssss}$ and tension $\mathbf{f}_{\text{ten}} = (\sigma \mathbf{x}_s)_s$, where s is the arclength, $\sigma = \Lambda - \frac{3}{2} \kappa^2$, Λ is the membrane tension, and κ is the membrane curvature (see Supplementary Material). Using $k_w \sim 10^{-12} \text{ m}^2\text{s/kg}$ and an osmolarity $\Delta c = 0.1 \text{ mol/L}$ (consistent with the osmotic filtration experiments (28)), the corresponding water flow is of the order $v_o = 0.1 \text{ } \mu\text{m/s}$. Assuming a membrane bending stiffness of $k_b = 10^{-19} \text{ J}$, a membrane tension of 10^{-3} N/m (one tenth of the lysis tension), and a characteristic length scale of 10^{-6} m , the tension contribution (v_t) and elastic stress contribution (v_e) to the permeable water flow can be scaled to v_o as $v_o : v_t : v_e = 10^0 : 10^{-2} : 10^{-6}$. Furthermore, we note that in the absence of an osmotic stress ($\Delta c = 0$), the permeating water flow may be non-negligible when the membrane tension becomes large due to the external stress such as the hydrodynamic stress from an external flow or confinement. In the following we explore both.

Specifically we focus on the mechanical component of the water flux in Eq. (1) with $\Delta c = 0$. In our non-dimensionalization the hydraulic conductivity is scaled to R_0/μ (where R_0 is a characteristic length and μ is the solvent viscosity): $\beta = k_w/(R_0/\mu)$ (see Supplementary Material), $\beta = 0$ for an impermeable vesicle, and $\beta > 0$ for a semipermeable vesicle. Under strong confinement, a large value of β is needed in our simulations to keep the membrane tension below the threshold value for membrane poration $\sim 10^{-3} \text{ N/m}$. Such large value of β may pertain to red blood cell membranes with aquaporin proteins.

Hydrodynamics of a semipermeable vesicle in free space

To highlight the effects of membrane permeability to water, we consider a single semipermeable vesicle, with (dimensionless) permeability coefficient $\beta > 0$, in familiar configurations: In free space we place a semipermeable vesicle in a quiescent flow, a planar shear flow, and a Poiseuille flow. For each example, we fix the vesicle length and examine the enclosed water content as a dynamic consequence of water flow, vesicle shape deformation, and membrane tension distribution. Under these flows, our simulations show that the steady state of an impermeable vesicle is different from that of a semipermeable vesicle, which depends only on the strength of the external flow and is insensitive to permeability β (as long as $\beta > 0$). We find that the time in the dynamic evolution towards equilibrium is scaled by β^{-1} : the smaller β is the longer it takes to reach the steady state.

In experiments, vesicles under shear flows are measured for a few minutes (chapter 19 in (26)), a duration over which a vesicle can be assumed impermeable (34). Our simulations of a semipermeable vesicle under these flows in open geometry show that water permeability may lead to different vesicle hydrodynamics only after a duration of ~ 1 day.

Quiescent Flow. In the absence of a background flow, a semipermeable vesicle in free space can be quantified in terms of its area dynamics and its transition to the equilibrium shape. Our analysis in Supplementary Material shows that

a semipermeable vesicle relaxes to a circle at a rate that is proportional to β , and the steady state tension is $\Lambda = 2\pi^2/L^2$. Our analysis further shows that the time for a semipermeable vesicle to deviate from its initial reduced area and to reach its steady state is proportional to β^{-1} . For this reason, our numerical results are reported in terms of the scaled time βt .

In Figure 2, we examine the relaxation dynamics of a semipermeable vesicle with four initial shapes and reduced areas as labeled. The vesicles on the left are color-coded by the water permeation flux: red denotes an influx into the vesicle, and blue denotes an efflux out of the vesicle. First we observe that the initial vesicle shape determines the direction of water flux. For the vesicle with an initial reduced area $\alpha(0) = 0.12$ (bottom row) the vesicle deflates (blue regions) first due to the high interior capillary pressure that corresponds to the high membrane curvatures. For the other three cases efflux is dominated by influx, especially after $t = 1$ day when the increase in total water content becomes non-negligible. Over time (about four weeks) all vesicles inflate and as expected, each vesicle eventually reaches a circular shape with reduced area $\alpha = 1$.

Between $t = 30$ minutes and $t = 1$ day, the total water content is nearly constant. This can be explained by considering the two terms that contribute to the vesicle velocity: (i) the permeability velocity, $\beta(\mathbf{f} \cdot \mathbf{n})\mathbf{n}$, and (ii) the force balance velocity, $\mathcal{S}[\mathbf{f}]$. Since $\beta \ll 1$, the permeability velocity is much smaller than the force balance velocity at early times, and the semipermeable vesicle dynamics resemble those of an impermeable vesicle. As the force balance velocity decreases, the permeability velocity dominates, and the vesicle begins to inflate to a circle with vanishing force and velocity.

Planar Shear Flow. We consider a semipermeable vesicle in a planar shear flow, characterized by the elastic capillary number $Ca_E = \chi\tau$ where τ is the characteristic time scale from balancing the viscous stress with the elastic stress (see Supplementary Material) and χ is the shear rate of the planar shear flow $\mathbf{u}_\infty(\mathbf{x}) = \chi(y, 0)$. When $\beta = 0$ (impermeable case), the vesicle reduced area and fluid viscosity contrast determine whether a vesicle tank treads or tumbles (35, 36). Focusing on semipermeable vesicles with no viscosity contrast, we find that a semipermeable vesicle tilts to an inclination angle and undergoes tank-treading dynamics, similar to the case of an impermeable vesicle.

In Figure 3(a), using four initial reduced areas and two flow rates, we plot the reduced area of a semipermeable vesicle with $\beta = 10^{-3}$. As observed in a quiescent flow, the final vesicle shape is independent of the initial reduced area. However, it does depend on the flow rate. We also observe that the amount of water inside the vesicle remains constant until $t \sim 2$ hours, when the normal component of the flow velocity becomes significantly smaller than the permeable velocity, leading to a changing reduced area.

For a variety of dimensionless permeability coefficient $\beta > 0$ and capillary number Ca_E , a semipermeable vesicle reaches an equilibrium shape as in Figure 3(a). Since the equilibrium shape depends on Ca_E and is independent of the initial reduced area, we initialize the vesicle with reduced area $\alpha = 0.65$ for all simulations in Figure 3(b), where we summarize the equilibrium vesicle shape and its reduced area. We see that the capillary number (flow rate) significantly affects the final vesicle shape, but the permeability coefficient has a very minor

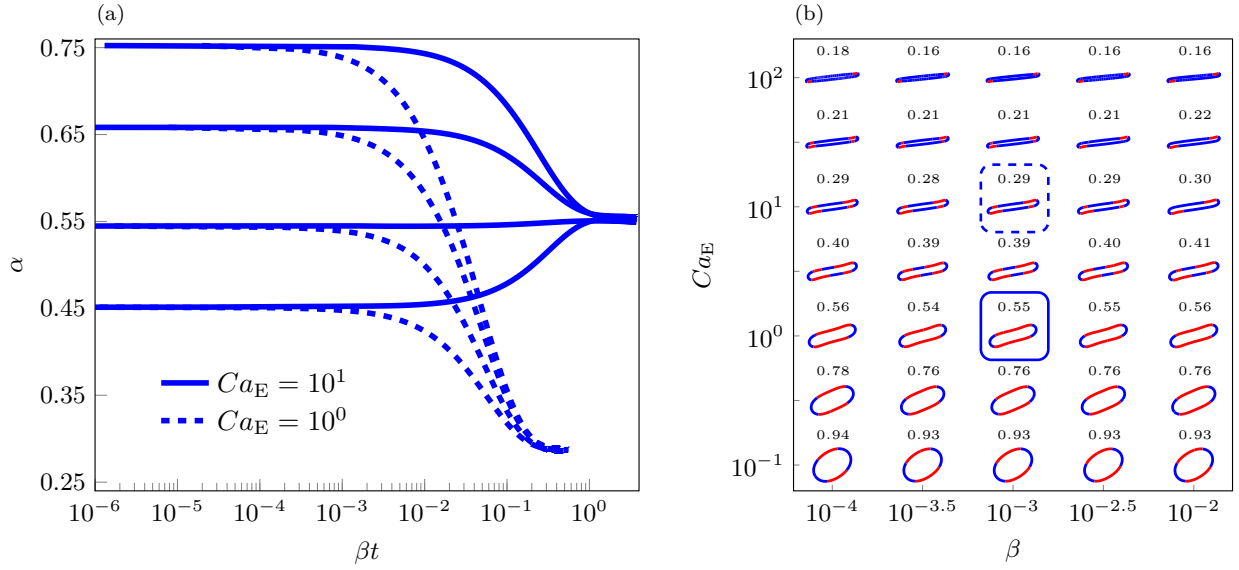


Fig. 3. (a) The reduced area of a semipermeable vesicle with $\beta = 10^{-3}$ initialized with four different reduced areas in a shear flow with two different flow rates. (b) The equilibrium shape of a vesicle with varying flow rates and membrane permeability. The circled vesicles correspond to the simulations in part (a).

effect. Instead, as we saw in the quiescent analysis, β sets a time scale since the time required for a vesicle to reach its steady state configuration is proportional to β^{-1} .

Poiseuille Flow. We consider a semipermeable vesicle in the Poiseuille flow $\mathbf{u} = U(1 - (y/W)^2, 0)$, where U is the maximum velocity at $y = 0$. The non-linear effects of the Poiseuille flow on the migration of an impermeable vesicle have been well-studied (37): At a given value of the maximum velocity U , there exists a critical reduced volume above which the equilibrium vesicle shape is symmetric (parachute or bullet shapes) and the vesicle stays at $y = 0$. Below this critical reduced volume the equilibrium vesicle moves off the center and is asymmetric (tank-treading slipper shape). We validated our numerical codes by comparing against results in Kaoui *et al.* (37) (see Supplementary Material).

At the beginning of the simulations, a semipermeable vesicle is placed above the center line $y = 0$ and it migrates towards the center line as in the impermeable case (38). Using several initial reduced areas and flow rates, we recreate the impermeable vesicle phase diagram for vesicles with $\beta = 10^{-3}$. The equilibrium vesicle shape for different U and initial reduced area is summarized in Figure 4(a), and the vertical displacement of the vesicle's center of mass is in Figure 4(b). The effect of semipermeability of a vesicle with $\alpha(0) = 0.9$ and $U = 800 \mu\text{m/s}$ on its reduced area and migration pattern are shown in Figures 4(c) and 4(d), respectively.

As observed for the planar shear flow, the equilibrium reduced area of a semipermeable vesicle in a Poiseuille flow is independent of the initial reduced area and β , and larger maximum flow velocity U results in smaller equilibrium reduced area (Figure 4(a)). At the smallest velocity $U = 200 \mu\text{m/s}$, the steady state reduced area is large, and the equilibrium vesicle shape is an axisymmetric bullet. The equilibrium reduced area decreases with increasing U , and the nonlinear flow profile gives rise to an asymmetric tank-treading slipper for $U \geq 400 \mu\text{m/s}$. We observe that the membrane permeability to water drastically alters the equilibrium vesicle shape and position

relative to the Poiseuille flow: At $\beta = 10^{-3}$ the equilibrium vesicle depends only on the maximum velocity U of the non-linear shear flow. The higher U the smaller the equilibrium reduced area and the farther away the vesicle is relative to the flow center at $y = 0$.

A semipermeable vesicle under strong confinement

Here we consider a semipermeable vesicle under strong confinement: a long closely-fit channel and a contracting channel. In a narrow microfluidic channel, a large pressure jump is often needed to push the vesicle through a closely-fit channel (39). Our simulations show that such a configuration can lead to an amplification of water permeation at a time scale shorter than a few minutes. In addition, we find that a large value of β is needed to keep the membrane tension below the threshold value for membrane poration. Such high permeability for water may be regarded as an indication that the lipid bilayer membrane is porated under strong confinement, and our model vesicle is for a porated vesicle within the Helfrich free energy framework. As in the previous examples, we fix the vesicle length and examine the enclosed water content as a dynamic consequence of water flow, vesicle shape deformation, and membrane tension distribution.

Semipermeable Vesicle in a Closely-fit Channel (Stenosis).

When red blood cells go through small capillary vessels, they experience large shape deformation and significant membrane stretching that triggers ATP release (14, 15). Many cells exhibit extraordinary flexibility as they go through narrow vessels (40), and adjustment of surface-to-volume ratio may be a key factor for a successful passage. Here we quantify the effect of water permeability on a vesicle going through a stenosis (a long microfluidic channel with a width smaller than the cell radius). Based on the findings in (39), we first examine the effect of semipermeability on the pressure fluctuation across a stenosed geometry. In this experiment, a pressure drop is used to squeeze a red blood cell through a constriction

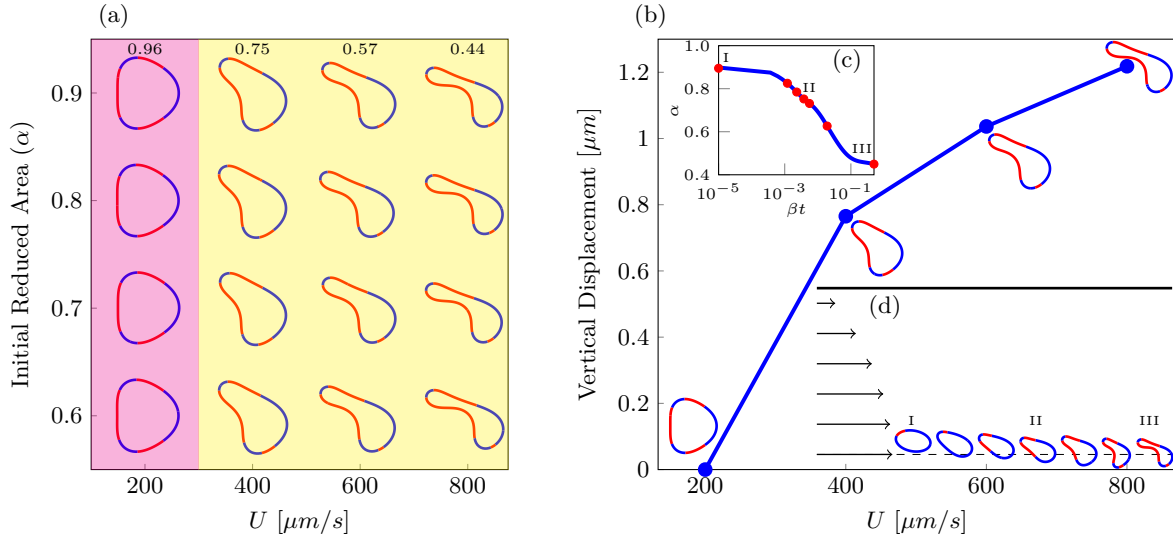


Fig. 4. (a) The equilibrium shape of a semipermeable vesicle submerged in a Poiseuille flow with varying initial reduced areas and flow rates. The red regions correspond to influx and the blue regions correspond to efflux. (b) The steady state vertical displacement at four different flow velocities. The steady state shapes are superimposed. (c) The reduced area of the slipper formed with the flow rate of 800 $\mu\text{m/s}$. (d) The vesicle shape shown with the background imposed flow. The channel width is 12.5 times larger than the vesicle radius. The corresponding reduced area of each vesicle is indicated by the marks in plot (c).

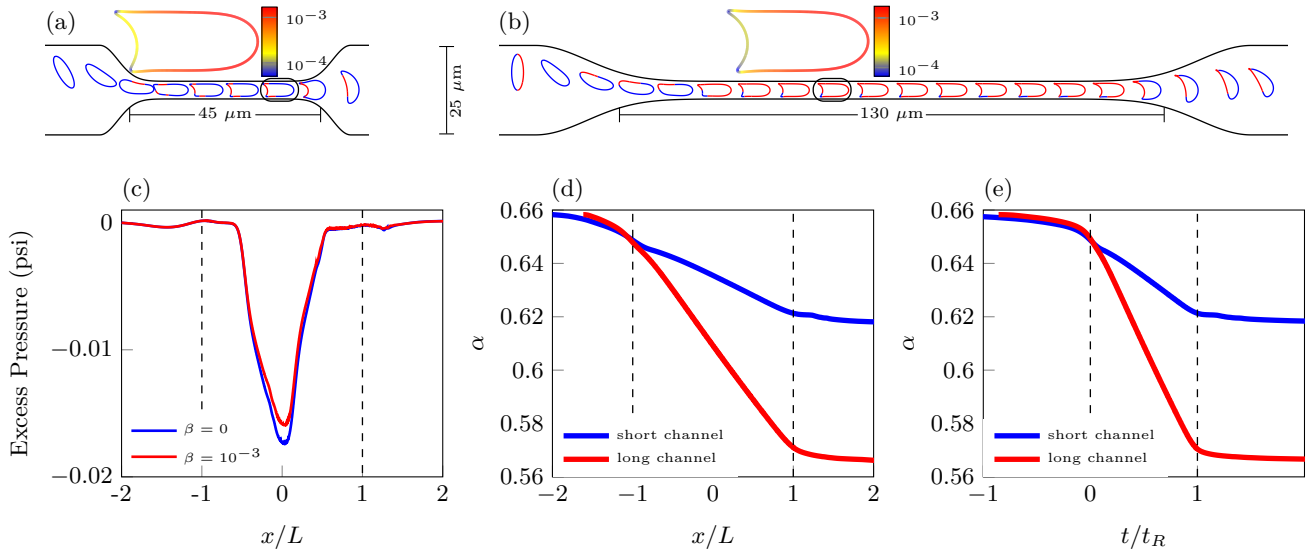


Fig. 5. (a) A semipermeable vesicle passing through a closely-fit channel similar to the experimental device in (39). (b) A semipermeable vesicle passing through a (four-times) longer closely-fit channel than (a). (c) The excess pressure of an impermeable and semipermeable vesicle in the short geometry in (a). (d) The reduced area of the semipermeable vesicles in the geometries in (a) and (b) as a function of the vesicles' center of mass. In (c) and (d), the x-axis is scaled by $1/L$ where L is half the length of the constriction. (e) The reduced area of the semipermeable vesicles in the geometries in (a) and (b) as a function of time. The time axis is scaled by $1/t_R$ where t_R is the residency time. In parts (c) and (d), the dashed lines correspond to the locations of the inlet and outlet. In part (e), the dashed lines correspond to the times that the vesicle enters and exits the constriction. The colored vesicles show the tension distribution in N/m of the circled vesicles. Throughout the entire simulation, these vesicle configurations have the largest tension.

with diameter $5 \mu\text{m}$ and length $45 \mu\text{m}$. We set up a similar computational geometry with a Poiseuille flow imposed at the inlet and outlet (Figure 5(a)). We set the maximum flow velocity to $U_{\text{max}} = 1000 \mu\text{m/s}$ at the inlet and outlet so that the residency time of the vesicle in the stenosis channel is $t_R \approx 25 \text{ ms}$ which agrees with the experimental results (39). When the red blood cell enters the channel, an increase in the pressure drop is required to maintain a constant flow rate, and the difference in the pressure drop is called the excess pressure.

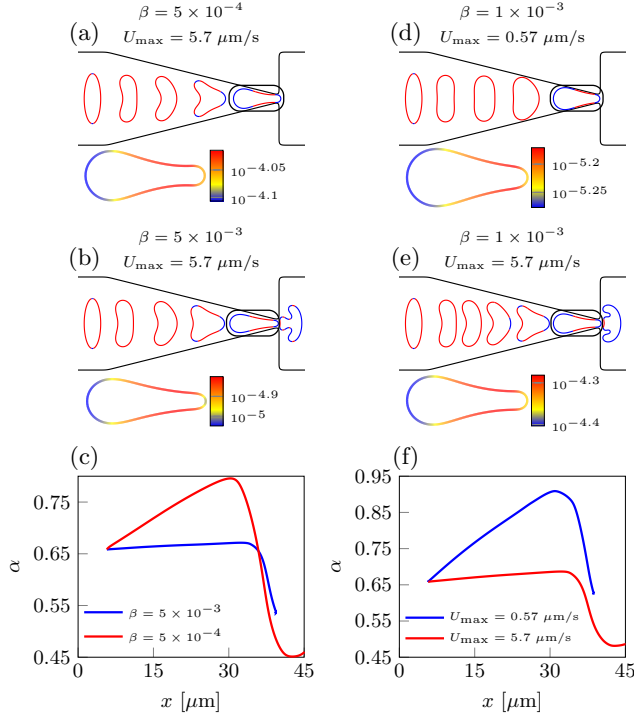


Fig. 6. A contracting channel similar to the experimental configuration in (41). The channel width varies from $18 \mu\text{m}$ to $1.8 \mu\text{m}$, and it repeats every $45 \mu\text{m}$. The fluid flux along the red regions is into the vesicle, and the fluid flux along the blue regions is out of the vesicle. (a–c): The ability for a semipermeable vesicle to pass through the contraction depends on the permeability β . (d–f): The ability for a semipermeable vesicle to pass through the contraction depends on the flow rate. The colored vesicles show the tension distribution in N/m of the circled vesicles. Throughout the entire simulation, these vesicle configurations have the largest tension.

We consider both an impermeable and semipermeable vesicle with initial reduced area $\alpha = 0.65$ passing through a long narrow channel and compute the excess pressure as a function of vesicle position in the channel (Figure 5(c)). The impermeable case agrees with experimental results (39) (see Figure 3). Our simulations show that less excess pressure is needed to drive a semipermeable vesicle through the closely-fit channel. Once in the channel, the vesicle takes a bullet shape with maximum tension in the front and minimum tension in the back (Figure 5(a)), consistent with earlier results (19, 42).

Figures 5(d) and 5(e) show that the vesicle deflates from the beginning due to the high flow velocity, consistent with the results for a vesicle in a Poiseuille flow in open space. As the vesicle enters the stenosis channel, it continues to deflate in the front even though we observe influx (red segment) at various rear locations in the membrane. Overall, the vesicle loses about 6.1% of its initial total water at a constant rate

as shown in Figures 5(d) and 5(e) (blue curves). Thus we expect that a larger amount of deflation is possible if the vesicle is inside a longer stenosis: we consider a vesicle passing through a channel of triple the length in Figure 5(b) with $U_{\text{max}} = 1000 \mu\text{m/s}$, and we observe that vesicle stays inside the stenosis for a residence time $t_R \approx 70 \text{ ms}$ and the area decreases by 13.2% (red curves).

Semipermeable Vesicle in a Contracting Geometry. Squeezing a cell or an elastic vesicle through a slit in microfluidics has gained popularity for its application in stress-induced release of macromolecules (17, 42–44). Red blood cells go through submicron slits many times during their lifetime, and this process selects healthy, flexible red blood cells to survive (41, 45). Here we investigate the role of membrane permeability to water when a semipermeable vesicle is squeezed through a contracting microfluidic channel similar to (41), where the width of the channel gradually decreases from $18 \mu\text{m}$ to $1.8 \mu\text{m}$. The channel then immediately reopens to $18 \mu\text{m}$ (Figure 6). A Poiseuille flow is imposed at the inlet and outlet with a constant maximum flow rate of U_{max} . We initialize a semipermeable vesicle with $\alpha = 0.65$ that spans $10 \mu\text{m}$ of the total channel width and investigate the effects of the membrane permeability to water and the maximum flow velocity on whether a vesicle can successfully pass through the slit. We color the vesicle according to the sign of its flux—red for influx and blue for efflux.

In Figures 6(a) and 6(b), we plot snapshots of vesicles with different permeability β . Figure 6(c) shows the corresponding reduced area as a function of the vesicle's location. We observe that if the permeability is sufficiently large, the vesicle inflates gradually over seconds before it reaches the neck, and then it quickly deflates within a fraction of a second. However, if the permeability β is too low, the vesicle is too large when it reaches the narrowest part of the channel, and it is unable to pass. In Figures 6(d) and 6(e), we plot snapshots of vesicles with different imposed maximum velocities, and Figure 6(f) shows the reduced area as a function of the vesicle's location. At low velocities, the vesicle inflates similar to the unbounded parabolic flow example, and it is unable to pass through the contraction. However, higher flow rates result in additional deflation and the vesicle passes through the contraction.

To understand the effects of water permeability on a vesicle that repeatedly passes through micro-capillary vessels or submicron slits, we construct a contracting geometry (Figure 7) to simulate a vesicle passing through the contracting geometry six times. In Figure 7(b), we show that the vesicle deflates each time it passes through the contraction followed by a gradual inflation (over seconds). The total area loss over the history of the vesicle is almost 50%. In Figure 7(c), we show the vesicle velocity as a function of the vesicle's center of mass. As the vesicle passes through the contraction, it first accelerates until it reaches the neck where it abruptly decelerates to go through the contraction. The reduced area and velocity with respect to time are also shown in Figure 7.

Discussion

In this work we investigate the effects of membrane permeability to water on vesicle hydrodynamics. Without any external flow or confinement, our analysis shows that a semipermeable vesicle always inflates to maximize the water content inside

the vesicle of a fixed length (area) in two (three) dimensions. Results from analysis and numerical simulation show that such relaxation of a semipermeable vesicle is characterized by a rescaled time βt . We further illustrate that the relaxation process consists of at least two phases: The first phase is dominated by the balance between membrane traction and viscous stress at early times (up to five minutes), when the vesicle behaves like an impermeable membrane. The second phase sets in after a few hours, when water influx begins to dominate and inflate the vesicle. Over a time scale of more than four weeks, a semipermeable vesicle is fully inflated, independent of its initial surface-to-volume ratio.

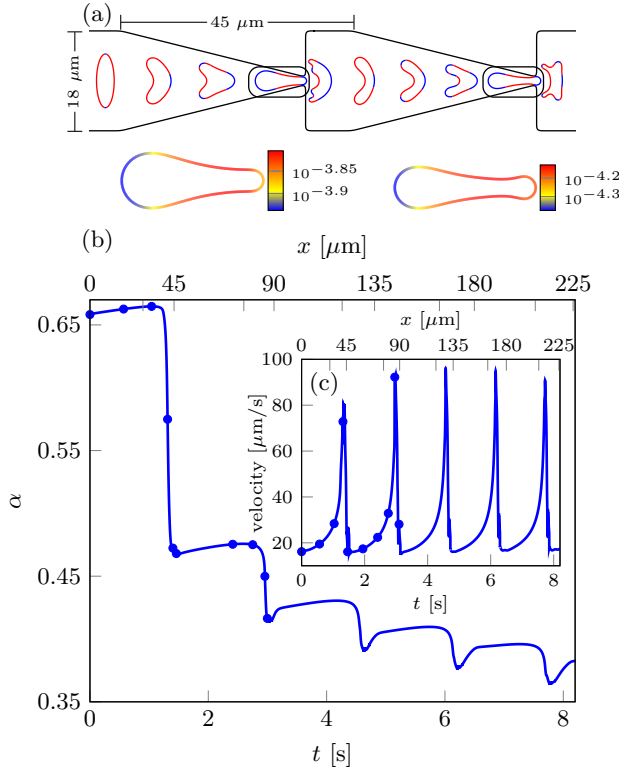


Fig. 7. Vesicle reduced area and velocity vs. time. The permeability coefficient is $\beta = 10^{-3}$ and the maximum velocity is 18 $\mu\text{m/s}$. (a) A semipermeable vesicle passing through six periods of the contracting geometry. (b) The reduced area with the marks representing shapes in (a). (c) The vesicle velocity with the marks representing shapes in (a). In (b) and (c), the lower x-axis is the x-coordinate of the center of mass, and the upper x-axis is time. The colored vesicles show the tension distribution in N/m of the circled vesicles. Throughout the entire simulation, these vesicle configurations have the largest tension.

Under strong confinement we show that water permeation can be amplified on a time scale of a few seconds as a vesicle is squeezed through a closely-fit channel and a contracting channel. As a semipermeable vesicle goes through a long closely-fit channel, we observe that the vesicle loses water at a constant rate, and the longer the channel the more the loss of water. In the case of a contracting channel, we find that both permeability and the pressure gradient across the slit must be sufficiently large for a successful passage. Throughout these simulations the membrane tension is below the threshold for membrane poration. Thus we expect the continuum membrane theory to well-capture the vesicle hydrodynamics, and our simulation results shed light on the configuration and time

scales needed to observe the effects of permeability on vesicle hydrodynamics under confinement.

Cells exhibit a dynamic volume-to-surface ratio in many physiological processes, such as cell migration in confined microenvironments (11, 46), dialysis (47), cell desiccation (48), cell division (49), and apoptosis (50). While osmotic stress is more effective and efficient than mechanical stress in contributing to change in cellular volume, our results suggest that the water permeation due to the capillary pressure may be non-negligible over long times or under strong confinement in simple configurations. To examine if this is the case in the physiological processes, currently we are examining the combined effects of osmotic and mechanical stresses on water permeation in the small Peclet number limit, which is relevant to cellular migration in the presence of both confinement and a solute gradient (11) and has been studied numerically by Jaeger *et al.* (51).

ACKNOWLEDGMENTS. We thank Howard Stone, Michael J. Shelley, Petia Vlahovska, Chaoqui Misbah, Manouk Abkarian, Sangwoo Shin, and Shravan K. Veerapaneni for discussions. B.Q. acknowledges support from the Simons Foundation, Mathematics and Physical Sciences-Collaboration Grants for Mathematicians, Award Number 527139. Y.-N.Y. acknowledges support from NSF (DMS 1614863, DMS 195160) and Flatiron Institute, part of Simons Foundation.

1. Cadart C, Venkova L, Recho P, Lagomarsino MC, Piel M (2019) The physics of cell-size regulation across timescales. *Nature Physics* 15:993–1004.
2. Alberts B, et al. (2015) Chapter 9 in *Molecular Biology of the Cell*. (Garland Science, Taylor & Francis Group, New York, New York, USA).
3. Yang B, Ma T, Verkman AS (2001) Erythrocyte water permeability and renal function in double knockout mice lacking aquaporin-1 and aquaporin-3. *J. Biol. Chem.* 276:624–628.
4. Sugie J, Intaglietta M, Sung LA (2018) Water transport and homeostasis as a major function of erythrocytes. *Am. J. Physiol. Heart Circ. Physiol.* 314:H1098–H1107.
5. Saadoun S, et al. (2005) Involvement of aquaporin-4 in astroglial cell migration and glial scar formation. *J. Cell Sci.* 118(24):5691–5698.
6. Verkman AS, Hara-Chikuma M, Papadopoulos M (2008) Aquaporins-new players in cancer biology. *J. Mol. Med.* 86:523–529.
7. Berthaud A, et al. (2016) Spreading of porous vesicles subjected to osmotic shocks: the role of aquaporins. *Soft Matt.* 12:1601.
8. Keren K (2011) Cell motility: the integrating role of the plasma membrane. *Eur. Biophys. J.* 40:1013–1027.
9. Taloni A, et al. (2015) Volume changes during active shape fluctuations in cells. *Phys. Rev. Lett.* 114:208101.
10. Jiang H, Sun SX (2013) Cellular Pressure and Volume Regulation and Implications for Cell Mechanics. *Biophys. J.* 105:609–619.
11. Stroka KM, et al. (2014) Water Permeation Drives Tumor Cell Migration in Confined Microenvironments. *Cell* 157:611–623.
12. Li Y, Mori Y, Sun SX (2015) Flow-Driven Cell Migration under External Electric Fields. *Phys. Rev. Lett.* 115:268101.
13. Yao L, Mori Y (2017) A numerical method for osmotic water flow and solute diffusion with deformable membrane boundaries in two spatial dimension. *Journal of Computational Physics* 350:728–746.
14. Wan J, Ristenpart WD, Stone HA (2008) Dynamics of shear-induced ATP release from red blood cells. *Proc. Nat. Sci. Acad.* 105(43):16432–16437.
15. Forsyth AM, Wan J, Owrutsky PD, Abkarian M, Stone HA (2011) Multiscale approach to link red blood cell dynamics, shear viscosity, and ATP release. *Proc. Nat. Acad. Sci.* 108(27):10986–10991.
16. Russell-Puleri S, et al. (2016) Fluid shear stress induces upregulation of COX-2 and PGI2 release in endothelial cells via a pathway involving PECAM-1, PI3K, FAK, and p38. *Am. J. Physiol. Heart Circ. Physiol.* 312:H485–H500.
17. Zhang H, Shen Z, Hogan B, Barakat AI, Misbah C (2018) ATP Release by Red Blood Cells under Flow: Model and Simulations. *Biophysical Journal* 115:2218–2229.
18. Gordon E, Schimmel L, Frye M (2020) The importance of Mechanical Forces for *in vitro* Endothelial Cell Biology. *Frontiers in Physiology* 11:684.
19. Harman A, Bertrand M, Joos B (2017) Deformation and rupture of vesicles confined in narrow channels. *Canadian Journal of Physics* 95:916–922.
20. Razizadeh M, Nikfar M, Paul R, Liu Y (2020) Coarse-Grained Modeling of Pore Dynamics on the Red Blood Cell Membrane under Large Deformations. *Biophys. J.* 119:471–482.
21. Dick DAT (1964) The Permeability Coefficient of Water in the Cell Membrane and the Diffusion Coefficient in the Cell Interior. *J. Theoret. Biol.* 7:504–531.
22. Fettilplace R, Haydon DA (1980) Water permeability of lipid membranes. *Physiological Reviews* 60(2):510–550.
23. Deamer DW, Bramhall J (1986) Permeability of lipid bilayers to water and ionic solutes. *Chem. Phys. Lipids* 40:167–188.

24. Grafmüller A (2019) Multiscale (re)modeling of lipid bilayer membranes. *Adv. Biomem. Lipid Self-Assembly* 30:1–66.
25. Thompson TE, Huang C (1966) The water permeability of lipid bilayer membranes. *Ann. N. Y. Acad. Sci.* 137:740–744.
26. Ugarte-Urbe B, Garcia-Saez AJ, Claessens MMAE (2019) Chapter 20: Membrane permeability measurements in *The Giant Vesicle Book*, eds. Dimova R, Marques C. (CRC Press).
27. Bhatia T, Robinson T, Dimova R (2020) Membrane permeability to water measured by microfluidic trapping of giant vesicles. *Soft Matt.* 16:7359.
28. Olbrich K, Rawicz W, Needham D, Evans E (2000) Water Permeability and Mechanical Strength of Polyunsaturated Lipid Bilayers. *Biophys. J.* 79:321–327.
29. Marrink SJ, Berendsen HJC (1994) Simulation of water transport through a lipid membrane. *J. Phys. Chem.* 98:4155–4168.
30. Oglecka K, Rangamani P, Liedberg B, Kraut RS, Parikh AN (2014) Oscillatory phase separation in giant lipid vesicles induced by transmembrane osmotic differentials. *eLife* 3:e03695.
31. Campos CV, Saric A (2020) Dynamics of vesicle reshaping and scission under osmotic shocks. *Soft Matt.* submitted.
32. Bhatia T, Christ S, Steinkuhler J, Dimova R, Lipowsky R (2020) Simple sugars shape giant vesicles into multispheres with many membrane necks. *Soft Matt.* 16:1246.
33. Minetti C, Callens N, Coupier G, Podgorski T, Dubois F (2008) Fast measurements of concentration profiles inside deformable objects in microflows with reduced spatial coherence digital holography. *Applied Optics* 47(29):5305–5314.
34. Abkarian M, Viallat A (2005) Dynamics of Vesicles in a Wall-Bounded Shear Flow. *Biophys. J.* 89:1055–1066.
35. Finken R, Lamura A, Seifert U, Gompper G (2008) Two-dimensional fluctuating vesicles in linear shear flow. *The European Physical Journal E* 25:309–321.
36. Kraus M, Wintz W, Seifert U, Lipowsky R (1996) Fluid Vesicles in Shear Flow. *Physical Review Letter* 77(17):3685–3688.
37. Kaoui B, Biros G, Misbah C (2009) Why Do Red Blood Cells Have Asymmetric Shapes Even in a Symmetric Flow? *Physical Review Letters* 103(18):188101.
38. Danker G, Vlahovska PM, Misbah C (2009) Vesicles in Poiseuille Flow. *Physical Review Letters* 102:148102.
39. Abkarian M, Faivre M, Stone HA (2006) High-speed microfluidic differential manometer for cellular-scale hydrodynamics. *Proceedings of the National Academy of Sciences* 103(3):538–542.
40. Au SH, et al. (2016) Clusters of circulating tumor cells traverse capillary-sized vessels. *Proc. Nat. Acad. Sci.* 113(18):4947–s4952.
41. Wu T, Guo Q, Ma H, Feng JJ (2015) The critical pressure for driving a red blood cell through a contracting microfluidic channel. *Theoretical and Applied Mechanics Letters* 5(6):227–230.
42. Pak OS, Young YN, Marple GR, Veerapaneni S, Stone HA (2015) Gating of a mechanosensitive channel due to cellular flows. *Proc. Nat. Acad. Sci.* 112(32):9822–9827.
43. Sharei A, et al. (2013) A vector-free microfluidic platform for intracellular delivery. *Proc. Nat. Acad. Sci.* 110(6):2082–2087.
44. Luo ZY, Bai BF (2019) Solute release from an elastic capsule flowing through a microfluidic channel constriction. *Phys. Fluids* 31:121902.
45. Lu H, Peng Z (2019) Boundary integral simulations of a red blood cell squeezing through a submicron slit under prescribed inlet and outlet pressures. *Phys. Fluids* 31:031902.
46. Papadopoulos MC, Saadoun S, Verkman AS (2008) Aquaporins and cell migration. *Pflügers Archiv-European Journal of Physiology* 456(4):693–700.
47. Wniewski J (2006) Mathematical modeling of fluid and solute transport in hemodialysis and peritoneal dialysis. *Journal of Membrane Science* 274:24–37.
48. J. Vogl C, Miksis MJ, Davis SH, Salac D (2014) The effect of glass-forming sugars on vesicle morphology and water distribution during drying. *Journal of The Royal Society Interface* 11(99):20140646.
49. Odermatt PD, et al. (2020) Variations of intracellular density during the cell cycle arise from tip-growth regulation in fission yeast. *bioRxiv* p. 2020.10.21.349696.
50. Marchetti P, et al. (1996) Mitochondrial permeability transition is a central coordinating event of apoptosis. *The Journal of Experimental Medicine* 184(3):1155–1160.
51. Jaeger M, Carin M, Medale M, Tryggvason G (1999) The Osmotic Migration of Cells in a Solute Gradient. *Biophys. J.* 77:1357–1267.
52. Quaife B, Biros G (2014) High-volume fraction simulations of two-dimensional vesicle suspensions. *Journal of Computational Physics* 274:245–267.
53. Rahimian A, Veerapaneni SK, Biros G (2010) Dynamic simulation of locally inextensible vesicles suspended in an arbitrary two-dimensional domain, a boundary integral method. *Journal of Computational Physics* 229:6466–6484.
54. Lu L, Rahimian A, Zorin D (2017) Contact-aware simulations of particulate Stokesian suspensions. *Journal of Computational Physics* 347:160–182.
55. Veerapaneni SK, Gueyffier D, Zorin D, Biros G (2009) A boundary integral method for simulating the dynamics of inextensible vesicles suspended in a viscous fluid in 2D. *Journal of Computational Physics* 228(7):2334–2353.
56. Alpert BK (1999) Hybrid Gauss-Trapezoidal Quadrature Rules. *SIAM Journal on Scientific Computing* 20:1551–1584.
57. Quaife B, Biros G (2016) Adaptive time stepping for vesicle simulations. *Journal of Computational Physics* 306:478–499.
58. Veerapaneni SK, Raj R, Biros G, Purohit PK (2009) Analytical and numerical solutions for shapes of quiescent two-dimensional vesicles. *International Journal of Non-Linear Mechanics* 44:257–262.
59. Ryham RJ (2018) On the viscous flows of leak-out and spherical cap natation. *Journal of Fluid Mechanics* 836:502–531.
60. Lai MC, Tseng YH, Huang H (2008) An immersed boundary method for interfacial flows with insoluble surfactant. *Journal of Computational Physics* 227:7279–7293.

Supplementary Material: Formulation

We consider a two-dimensional inextensible semipermeable vesicle membrane γ suspended in a viscous Newtonian fluid in domain Ω . The vesicle membrane γ is parameterized as $\mathbf{x}(s, t)$ where s is arclength and t is time. In the suspending fluid the flow velocity \mathbf{u} and pressure p are governed by the incompressible Stokes equations

$$-\nabla p + \mu \Delta \mathbf{u} = 0, \quad \nabla \cdot \mathbf{u} = 0, \quad \mathbf{x} \in \Omega \setminus \gamma, \quad [2]$$

where μ is the fluid viscosity. When Ω is an unconfined geometry, the condition $\mathbf{u}(\mathbf{x}) \rightarrow \mathbf{u}_\infty(\mathbf{x})$ as $|\mathbf{x}| \rightarrow \infty$ is enforced. In the confined examples, we enforce a no-slip boundary condition along the top and bottom of the channel and a Hagen–Poiseuille flow at the inlet and outlet—this boundary condition has been used in similar vesicle setups (52–54). Along the vesicle membrane γ , mass continuity, force balance, and local inextensibility are enforced by requiring

$$[\mathbf{u}]_\gamma = 0, \quad [T \cdot \mathbf{n}]_\gamma = \mathbf{f}_{\text{mem}}, \quad \mathbf{x}_s \cdot \mathbf{u}_s = 0, \quad [3]$$

where \mathbf{n} is the outward normal of γ , $[\cdot]_\gamma$ is the jump across the interface, and T is the hydrodynamic stress tensor. The membrane force \mathbf{f}_{mem} is the sum of a bending force with bending modulus k_b and a force due to the tension Λ . Following (55), we introduce the variable $\sigma = \Lambda - \frac{3}{2}\kappa^2$, where κ is the vesicle curvature. Then, the bending and tension forces corresponding to the Helfrich energy are $\mathbf{f}_{\text{ben}} = -k_b \mathbf{x}_{ssss}$ and $\mathbf{f}_{\text{ten}} = (\sigma \mathbf{x}_s)_s$.

Semipermeability is introduced by modifying the vesicle velocity from the standard no-slip condition $\dot{\mathbf{x}} = \mathbf{u}(\mathbf{x})$. Instead, the permeating water flux through the lipid bilayer membrane is proportional to the membrane traction (13). That is,

$$\mathbf{u} - \dot{\mathbf{x}} = -k_w (\mathbf{f}_{\text{mem}} \cdot \mathbf{n}) \mathbf{n}, \quad \mathbf{x} \in \gamma, \quad [4]$$

where k_w is the hydraulic conductivity.

The governing equations are non-dimensionalized by using a characteristic length scale $R_0 = 10^{-6}$ m, a bending stiffness $k_b = 10^{-19}$ J, and fluid viscosity 5×10^{-2} kg/ms. We scale time by $\tau = \mu R_0^3 / k_b = 0.5$ s, the velocity by $R_0 / \tau = 2$ $\mu\text{m/s}$, the pressure by $k_b / R_0^3 = 10^{-1}$ Pa, the tension by $k_b / R_0^2 = 10^{-7}$ N/m, and the permeability by $R_0 / \mu = 10^{-3}$ m²s/kg. Under this nondimensionalization, a two-dimensional semipermeable vesicle in a viscous fluid is characterized by (a) its reduced area $\alpha = 4\pi A / L^2 \in (0, 1]$, where L is the vesicle length and A is its area, and (b) its permeability $\beta = k_w \mu / R_0$. In two dimensions, the membrane length is conserved by the local inextensibility condition, but the enclosed area is not conserved because of semipermeability. Therefore, the reduced area is dynamic. We convert the apparent permeability of a polyunsaturated PC bilayer (28) to the hydraulic conductivity k_w using the conversion in (22), and found that $10^{-14} \leq k_w \leq 10^{-12}$ m²s/kg, thus β is in the range $10^{-11} \leq \beta \leq 10^{-9}$.

Since the fluid satisfies the Stokes equations, the velocity and pressure can be represented as layer potentials. Given the interfacial boundary conditions Eq. (3), the fluid velocity is

$$\mathbf{u}(\mathbf{x}) = \mathbf{u}_\infty(\mathbf{x}) + \mathcal{S}[\mathbf{f}_{\text{mem}}](\mathbf{x}), \quad \mathbf{x} \in \Omega, \quad [5]$$

where \mathcal{S} is the single-layer potential

$$\mathcal{S}[\mathbf{f}](\mathbf{x}) = \frac{1}{4\pi} \int_\gamma \left(-\mathbf{I} \log \rho + \frac{\mathbf{r} \otimes \mathbf{r}}{\rho^2} \right) \mathbf{f}(\mathbf{y}) d\mathbf{y}_y, \quad [6]$$

with $\mathbf{r} = \mathbf{x} - \mathbf{y}$ and $\rho = |\mathbf{r}|$. Imposing the flux condition Eq. (4) and the inextensibility condition, the vesicle velocity satisfies the boundary integral equation

$$\dot{\mathbf{x}} = \mathbf{u}_\infty(\mathbf{x}) + \beta (\mathbf{f}_{\text{mem}} \cdot \mathbf{n}) \mathbf{n} + \mathcal{S}[\mathbf{f}_{\text{mem}}](\mathbf{x}), \quad \mathbf{x}_s \cdot \dot{\mathbf{x}}_s = 0. \quad [7]$$

In confined geometries, the far field term $\mathbf{u}_\infty(\mathbf{x})$ is replaced by a double-layer potential with an unknown density defined on $\partial\Omega$. The density function is used to satisfy the boundary condition on $\partial\Omega$.

Supplementary Material: Numerical Methods

Discretization in Space. By using a boundary integral equation formulation, the unknowns are the vesicle's position and tension and the unknown density function for confined flows. Both γ and $\partial\Omega$ are discretized at a set of collocation points. Derivatives are computed with Fourier differentiation, and the eighth-order quadrature (56) is applied to the weakly singular single-layer potential.

For confined geometries, the trapezoid rule is used to approximate the double-layer potential since its kernel is smooth and periodic. Nearly-singular integrals are computed with an interpolation-based quadrature rule (52).

Discretization in Time. To eliminate stringent time step restrictions, we modify a time stepping method that discretizes high-order derivatives semi-implicitly (55). We introduce the notation

$$B[\mathbf{x}]\mathbf{f} = -\frac{d^4}{ds^4}\mathbf{f}, \quad T[\mathbf{x}]\sigma = (\sigma\mathbf{x}_s)_s, \quad [8]$$

$$D[\mathbf{x}]\mathbf{f} = \mathbf{x}_s \cdot \mathbf{f}_s, \quad P[\mathbf{x}]\mathbf{f} = (\mathbf{f} \cdot \mathbf{n})\mathbf{n}, \quad [9]$$

for the differential and projection operators. Then, the governing equations Eq. (7) are

$$\dot{\mathbf{x}} = \mathbf{u}_\infty(\mathbf{x}) + \beta P(B\mathbf{x} + T\sigma) + S(B\mathbf{x} + T\sigma), \quad D\dot{\mathbf{x}} = 0. \quad [10]$$

We note that the integral and differential operators, which all depend on the vesicle shape, are non-linear with respect to the vesicle shape. We construct a time stepping scheme by letting B^N be the bending operator due to the vesicle configuration at time t^N , and use similar notation for the other operators. Then, a first-order semi-implicit time stepping method of Eq. (7) is

$$\frac{\mathbf{x}^{N+1} - \mathbf{x}^N}{\Delta t} = \mathbf{u}_\infty(\mathbf{x}^N) + \beta P^N (B^N \mathbf{x}^{N+1} + T^N \sigma^{N+1}) + S^N (B^N \mathbf{x}^{N+1} + T^N \sigma^{N+1}), \quad [11]$$

$$D^N \mathbf{x}^{N+1} = 1, \quad [12]$$

and this linear system is solved with matrix-free GMRES.

To achieve second-order accuracy over long time horizons, we modify an adaptive spectral deferred correction time stepping method (57). Since the area of the vesicle is not conserved, we only use the length of the vesicle to estimate the error which determines if a time step is accepted or not and determines the subsequent time step size.

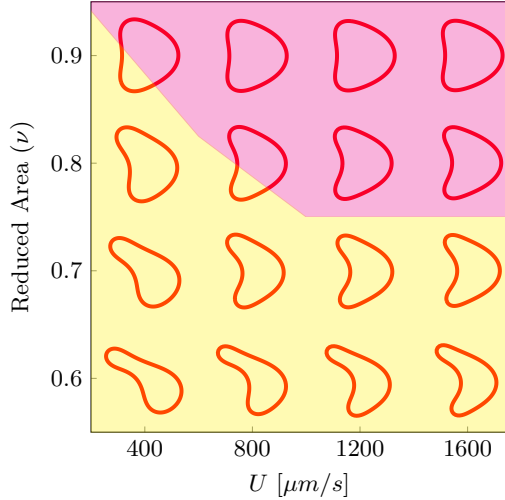


Fig. 8. Phase diagram of an impermeable vesicle with various reduced areas submerged in a Poiseuille flow with various flow rates. The shapes agree qualitatively with Kaoui *et al.* (37) (see Figure 2).

Numerical Validation. To validate our numerical codes for simulating vesicle hydrodynamics, we reproduce a phase diagram of the equilibrium shape of an impermeable vesicle in a Poiseuille flow. Depending on the maximum flow velocity and the vesicle reduced area, the equilibrium vesicle shape is either an axisymmetric bullet, an axisymmetric parachute, or a tank-treading asymmetric slipper (37). Comparing our results (Figure 8) with those in (37) (see Figure 2), we observe qualitative agreement in the equilibrium vesicle shapes except that, Kaoui *et al.* report that the vesicles with $\alpha = 0.7$ and flow rates $U = 1200 \mu\text{m/s}$ and $U = 1600 \mu\text{m/s}$ are axisymmetric.

In our simulations these vesicles are slightly asymmetric, are undergoing a tank-treading motion, and we therefore report them as asymmetric slippers.

Supplementary Material: Vesicle Area

In the absence of an imposed flow, the steady state vesicle shape and a differential equation for the area of the vesicle can be derived. We start by following the analysis of Veerapaneni *et al.* (58) by computing the steady state shape of a semipermeable vesicle in a quiescent flow. The steady state shape is a stationary point of the Lagrangian

$$\mathcal{L} = \frac{1}{2} \int_{\gamma} \kappa^2 ds + \Lambda \left(\int_{\gamma} ds - L \right), \quad [13]$$

where the Lagrange multiplier Λ is the tension. Note the absence of the pressure Lagrange multiplier since the total water content inside the vesicle membrane is not conserved. Taking the variation of \mathcal{L} with respect to γ and setting it to zero, the steady state shape satisfies $\kappa_{ss} + \frac{1}{2}\kappa^3 - \Lambda\kappa = 0$, with initial conditions $\kappa(0) = \kappa_0$ and $\kappa_s(0) = 0$. Integrating once, we have

$$\frac{\kappa_s^2}{2} + \frac{\kappa^4}{8} - \frac{\Lambda}{2}\kappa^2 = \frac{\kappa_0^4}{8} - \frac{\Lambda}{2}\kappa_0^2. \quad [14]$$

Assuming $\kappa_s \neq 0$, Eq. (14) is separable, and can be solved analytically in terms of the *EllipticF* function using Mathematica. Unlike in the impermeable case, the solution of Eq. (14) is not periodic unless $\kappa(s) = \kappa_0$. Therefore, the equilibrium shape of a semipermeable vesicle in a quiescent flow is a circle with radius $L/2\pi$ and constant tension $\Lambda = \kappa^2/2 = 2\pi^2/L^2$. Note that in contrast to an impermeable vesicle, the steady state tension is positive rather than negative. Such equilibrium shape of a semipermeable vesicle results from the balance between elastic stress and membrane tension. For an elastic membrane with a large pore, the equilibrium membrane (hemispherical) shape also results from such balance (59).

We next compute the transient area of the vesicle. Since the area of the vesicle is

$$A(t) = \frac{1}{2} \int_{\gamma} (\mathbf{x} \cdot \mathbf{n}) ds, \quad [15]$$

its derivative includes terms due to the time derivative of $\mathbf{x} \cdot \mathbf{n}$ and a term due to interface stretching (60), but this latter term is zero because of the local inextensibility condition. Therefore,

$$\dot{A}(t) = \frac{1}{2} \int_{\gamma} (\dot{\mathbf{x}} \cdot \mathbf{n}) ds + \frac{1}{2} \int_{\gamma} (\mathbf{x} \cdot \dot{\mathbf{n}}) ds. \quad [16]$$

Applying integration by parts, the two integrals agree, and we have

$$\dot{A}(t) = \int_{\gamma} (\beta(\mathbf{f} \cdot \mathbf{n})\mathbf{n} + S[\mathbf{f}]) \cdot \mathbf{n} ds = \beta \int_{\gamma} (\mathbf{f} \cdot \mathbf{n}) ds, \quad [17]$$

where we have used the incompressibility of the single-layer potential. Repeatedly applying integration by parts, we obtain

$$\dot{A}(t) = \beta \int_{\gamma} \left(\frac{\kappa^3}{2} - \kappa\Lambda \right) ds. \quad [18]$$

Note that the integrand in Eq. (18) is zero when the membrane tension balances the elastic force:

$$\Lambda = \frac{\kappa^2}{2} = \frac{\kappa_0^2}{2} \text{ at equilibrium,} \quad [19]$$

which is consistent with the equilibrium results in the vesicle area dynamics.

Supplementary Material: Vesicle Tensions

Vesicle Relaxation. Figure 9 shows the membrane tension distribution along the relaxing vesicles in Figure 2. The membrane tension magnitude (color bars) is in N/m. As the semipermeable vesicle relaxes, the membrane tension reduces in magnitude and becomes more evenly distributed along the membrane. In the top row ($\alpha(0) = 0.95$) the vesicle nearly relaxes to a circle on the right, and

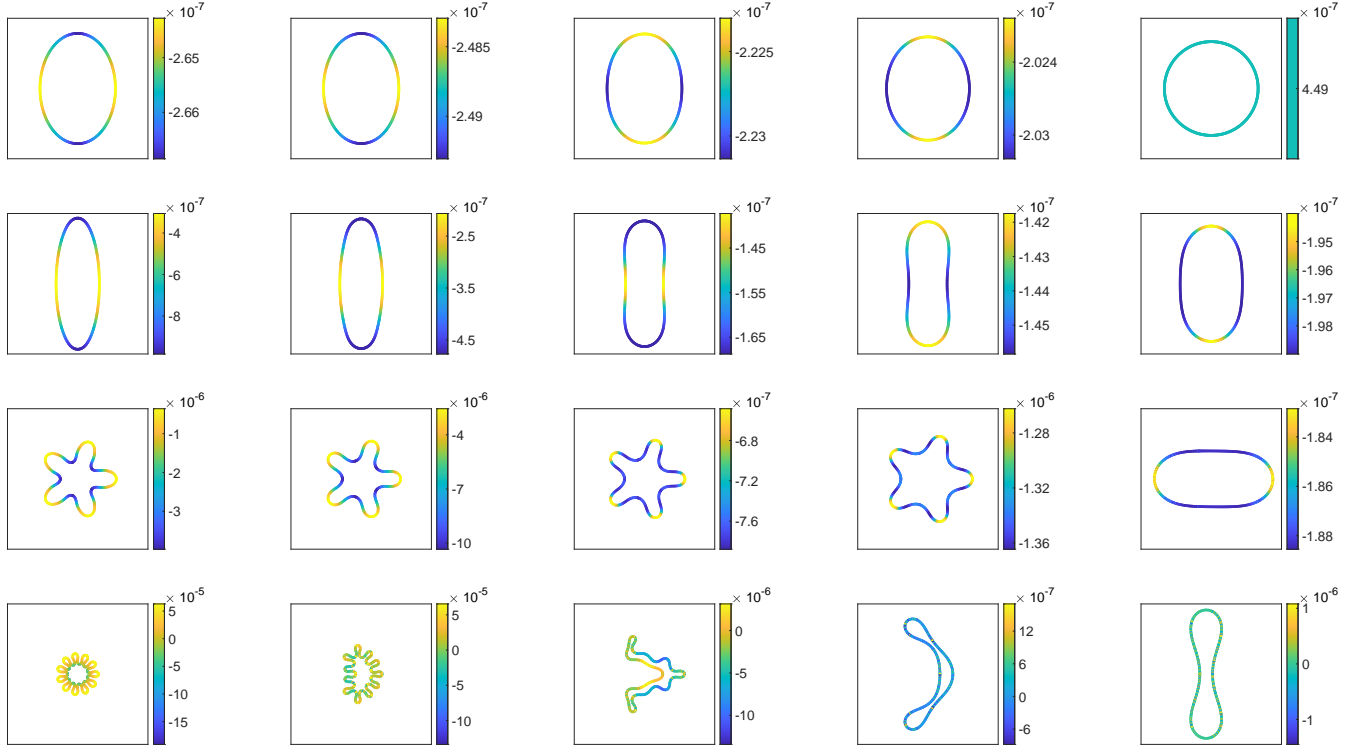


Fig. 9. The tension distribution of vesicles in relaxation that corresponds to Figure 2.

the membrane tension is uniform and equal to $k_b \kappa_0^2/2$ as predicted by our analysis (see Eq. (19)). In the bottom row ($\alpha(0) = 0.12$), the initial vesicle shape has a lot of high curvature regions (and thus the low reduced area), and it takes more than four hours to inflate to twice the initial total water content for $\beta = 10^{-7}$. In contrast the water enclosed inside the vesicle in the top row remains nearly constant in the first four hours.

Vesicle in a Planar Shear Flow. Our simulations of a semipermeable vesicle in a planar shear flow show that the equilibrium vesicle shape depends mostly on the capillary number Ca_E , independent of the dimensionless water permeability β . Our simulations show that the time it takes for a semipermeable vesicle to reach equilibrium in a planar shear flow is inversely proportional to β , just like the relaxing vesicle. The tension distribution along the equilibrium vesicle at $\beta = 10^{-4}$ is shown in Figure 10, where the color bars are for the membrane tension in N/m. The capillary number Ca_E increases from Figure 10(a) to (g), and we observe that the tension magnitude also increases almost linearly with Ca_E . We also observe that the membrane tension is relatively small at the tip when the membrane curvature is large due to the extensional component in the shear flow.

Vesicle in a Poiseuille flow. In a nonlinear shear flow, an impermeable vesicle can reach equilibrium position at the mid-plane of the shear flow for sufficiently large reduced area, regardless of the maximum flow velocity U . For a semipermeable vesicle, however, our simulation results (summarized in Figure 4) show that the equilibrium vesicle shape and position are determined by U , and independent

of the initial vesicle reduced area and permeability β . The corresponding membrane tension distribution is shown in Figure 11 as a function of flow velocity U from $200 \mu\text{m/s}$ to $800 \mu\text{m/s}$.

We note that in the Poiseuille flow the membrane tension is positive in the front, and negative in the rear part of the vesicle. Furthermore we also note that the tension magnitude is almost linearly proportional to U as in the linear shear flow.

Vesicle in a Closely-Fit Channel. When a semipermeable vesicle goes through a closely-fit channel, we observe that the water efflux is found in the front, and the influx is in the rear of the vesicle membrane (Figure 5). This corresponds well to the corresponding tension distribution in Figure 12: Larger tension in the front, and smaller tension in the rear.

Vesicle Going Through a Contracting Channel (Slit). When a semipermeable vesicle goes through a contracting channel (slit) the numerical simulations show that both the driving flow and the membrane permeability have to be sufficiently large for a successful passage through the slit (Figure 6). As the vesicle goes through the contracting channel, the gradual confinement first leads to a slow inflation. Once the vesicle is close to the neck, it quickly deflates in order to fit the constriction. When the vesicle is near the neck, simulations show that the water efflux is in the front and rear of vesicle while most water influx is in the middle. The tension distribution along the vesicle as a function of their position in the contracting channel is summarized in Figure 13, where we observe the tension has the largest magnitude when the vesicle is at the neck.

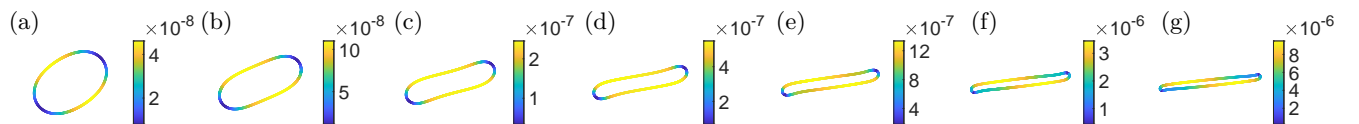


Fig. 10. The tension distribution along a vesicle in a linear shear flow. The semipermeability constant is $\beta = 10^{-4}$ for all these cases, and the elastic capillary number ranges from 10^{-1} to 10^2 as in Figure 3.

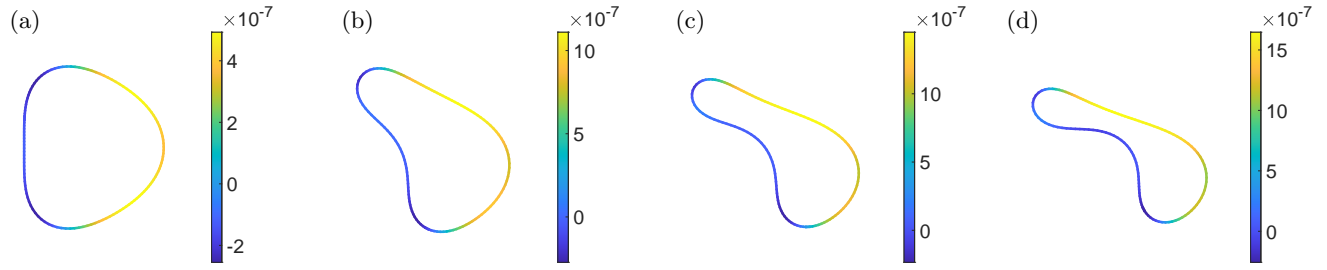


Fig. 11. The equilibrium tension distribution of a semipermeable vesicle with $\beta = 10^{-3}$ in a parabolic flow (Figure 4). The flow velocities are (a) 200 $\mu\text{m/s}$, (b) 400 $\mu\text{m/s}$, (c) 600 $\mu\text{m/s}$, and (d) 800 $\mu\text{m/s}$.

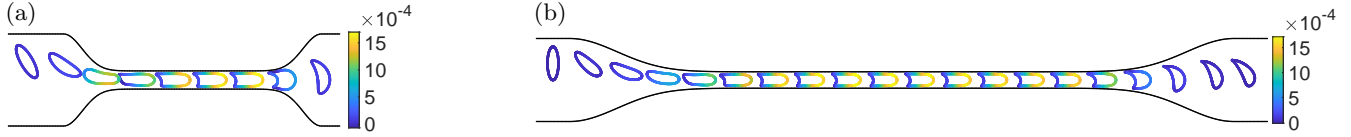


Fig. 12. The tension distribution along a semipermeable vesicle with $\beta = 10^{-3}$ going through a closely-fit channel of two different lengths.

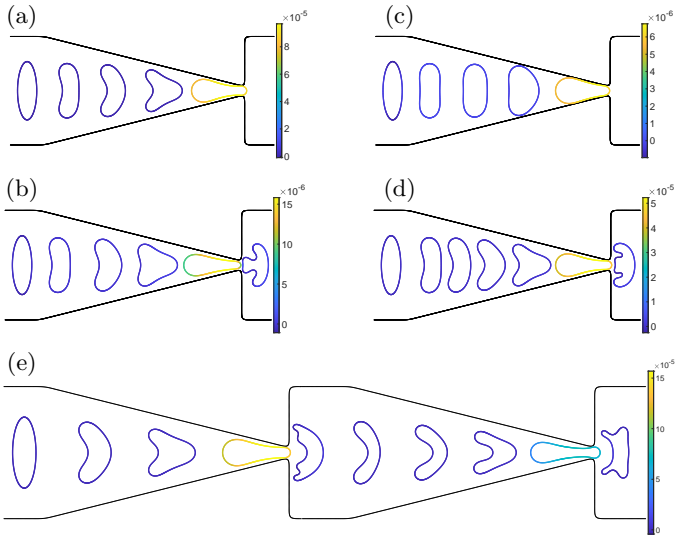


Fig. 13. The tension distribution along a semipermeable vesicle going through a contracting geometry. The vesicle tension increases by up to five orders of magnitude when as it enters the neck. The permeability constant and flow rates are (a) $U_{\text{max}} = 5.7 \mu\text{m/s}$, $\beta = 5 \times 10^{-4}$; (b) $U_{\text{max}} = 5.7 \mu\text{m/s}$, $\beta = 5 \times 10^{-3}$; (c) $U_{\text{max}} = 0.57 \mu\text{m/s}$, $\beta = 1 \times 10^{-3}$; (d) $U_{\text{max}} = 5.7 \mu\text{m/s}$, $\beta = 1 \times 10^{-3}$; (e) $U_{\text{max}} = 18 \mu\text{m/s}$, $\beta = 1 \times 10^{-3}$.